Report

Cell Reports

PIP4Ks Suppress Insulin Signaling through a Catalytic-Independent Mechanism

Graphical Abstract

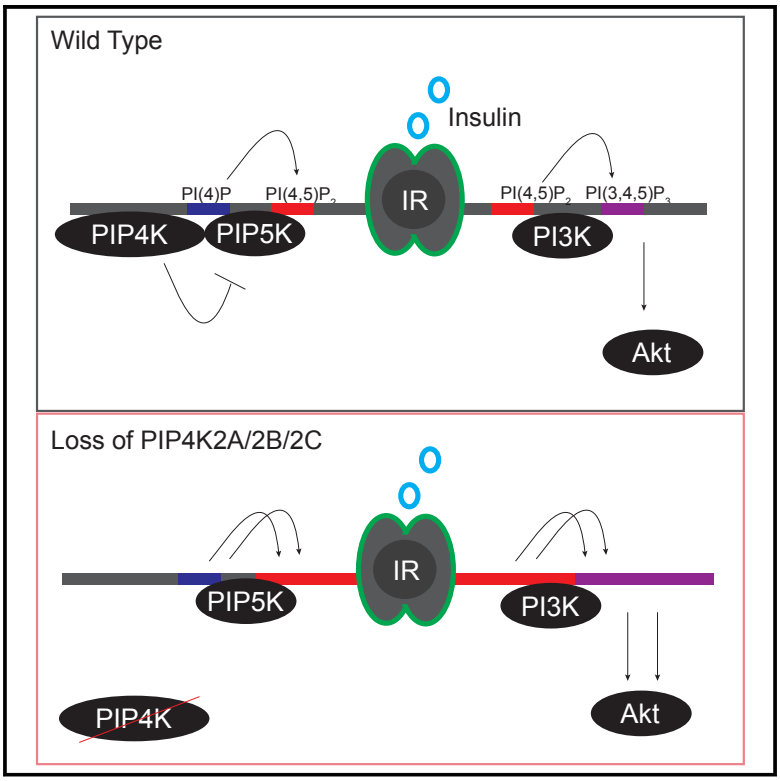

Authors

Diana G. Wang, Marcia N. Paddock, Mark R. Lundquist, ..., Jeremy M. Baskin, Lukas E. Dow, Lewis C. Cantley

Correspondence

lcantley@med.cornell.edu

In Brief

$PI(4,5)P_2$ is produced by both phosphatidylinositol-4-phosphate 5-kinases (PIP5Ks) and by phosphatidylinositol-5-phosphate 4-kinases (PIP4Ks). Wang et al. report an allosteric function of a conserved N-terminal motif of PIP4Ks in suppressing PIP5K-mediated $PI(4,5)P_2$ synthesis and insulin-dependent conversion to $PI(3,4,5)P_3$. This non-catalytic role has implications for the development of PIP4K targeted therapies.

Highlights

- PIP4Ks suppress PIP5K activity and insulin-stimulated production of $PI(3,4,5)P_3$
- PIP5K inhibition is independent of PIP4K catalytic activity
- PIP5K inhibition is dependent on the N-terminal motif VMLLPDD on PIP4K
- PIP4Ks have distinct catalytic and structural roles regulating metabolism

Wang et al., 2019, Cell Reports *27*, 1991–2001
May 14, 2019 © 2019 The Authors.
https://doi.org/10.1016/j.celrep.2019.04.070

CellPress

Cell Reports
Report

OPEN ACCESS
CellPress

PIP4Ks Suppress Insulin Signaling through a Catalytic-Independent Mechanism

Diana G. Wang,[1,2,7] Marcia N. Paddock,[1,3,7] Mark R. Lundquist,[1] Janet Y. Sun,[1] Oksana Mashadova,[1] Solomon Amadiume,[1] Timothy W. Bumpus,[4] Cindy Hodakoski,[1] Benjamin D. Hopkins,[1] Matthew Fine,[1] Amanda Hill,[1] T. Jonathan Yang,[1,5] Jeremy M. Baskin,[4] Lukas E. Dow,[1,3,6,8] and Lewis C. Cantley[1,8,*]

[1]Meyer Cancer Center, Weill Cornell Medicine, New York, NY 10021, USA
[2]Weill Cornell Medicine/Rockefeller University/Sloan Kettering Tri-Institutional MD-PhD Program, New York, NY 10021, USA
[3]Hematology and Oncology Division, Department of Medicine, Weill Cornell Medicine, New York, NY 10021, USA
[4]Department of Chemistry and Chemical Biology and Weill Institute for Cell and Molecular Biology, Cornell University, Ithaca, NY 14853, USA
[5]Department of Radiation Oncology, Memorial Sloan Kettering Cancer Center, New York, NY 10065, USA
[6]Department of Biochemistry, Weill Cornell Medicine, New York, NY 10021, USA
[7]These authors contributed equally
[8]Lead Contact
*Correspondence: lcantley@med.cornell.edu
https://doi.org/10.1016/j.celrep.2019.04.070

SUMMARY

Insulin stimulates the conversion of phosphatidylinositol-4,5-bisphosphate ($PI(4,5)P_2$) to phosphatidylinositol-3,4,5-trisphosphate ($PI(3,4,5)P_3$), which mediates downstream cellular responses. $PI(4,5)P_2$ is produced by phosphatidylinositol-4-phosphate 5-kinases (PIP5Ks) and by phosphatidylinositol-5-phosphate 4-kinases (PIP4Ks). Here, we show that the loss of PIP4Ks (*PIP4K2A, PIP4K2B*, and *PIP4K2C*) *in vitro* results in a paradoxical increase in $PI(4,5)P_2$ and a concomitant increase in insulin-stimulated production of $PI(3,4,5)P_3$. The reintroduction of either wild-type or kinase-dead mutants of the PIP4Ks restored cellular $PI(4,5)P_2$ levels and insulin stimulation of the PI3K pathway, suggesting a catalytic-independent role of PIP4Ks in regulating $PI(4,5)P_2$ levels. These effects are explained by an increase in PIP5K activity upon the deletion of PIP4Ks, which normally suppresses PIP5K activity through a direct binding interaction mediated by the N-terminal motif VMLΦPDD of PIP4K. Our work uncovers an allosteric function of PIP4Ks in suppressing PIP5K-mediated $PI(4,5)P_2$ synthesis and insulin-dependent conversion to $PI(3,4,5)P_3$ and suggests that the pharmacological depletion of PIP4K enzymes could represent a strategy for enhancing insulin signaling.

INTRODUCTION

Phosphatidylinositol-4,5-bisphosphate ($PI(4,5)P_2$) plays numerous roles in cellular regulation. It mediates actin remodeling at the plasma membrane, modulates vesicle trafficking, and is the substrate that hormone-stimulated phospholipases type C (PLC) use to generate the second messengers diacylglycerol and inositol-1,4,5-trisphosphate (Balla, 2013; Sun et al., 2013). $PI(4,5)P_2$ is also the substrate that class 1 phosphoinositide 3-kinases use (Saito et al., 2003) to generate the second messenger phosphatidylinositol-3,4,5-trisphosphate ($PI(3,4,5)P_3$) in response to insulin and other growth factors (Fruman et al., 2017).

Yeasts have a single enzyme for generating $PI(4,5)P_2$ encoded by *MSS4* (Homma et al., 1998), whereas mammals have six genes encoding enzymes that generate $PI(4,5)P_2$. *PIP5K1A*, *PIP5K1B*, and *PIP5K1C* produce $PI(4,5)P_2$ from phosphatidylinositol-4-phosphate (PI(4)P), while *PIP4K2A*, *PIP4K2B*, and *PIP4K2C* generate $PI(4,5)P_2$ from phosphatidylinositol-5-phosphate (PI(5)P) (Rameh et al., 1997; van den Bout and Divecha, 2009). All multicellular organisms have genes from both families. The enzymes encoded by these two families of genes have sequence and structural similarities, but the activation loop of the PIP4Ks confers strict substrate selectivity for PI(5)P over PI(4)P (Kunz et al., 2000, 2002).

In settings where phosphoinositides have been quantified, PI(4)P and $PI(4,5)P_2$ each constitute between 30% and 50% of total cellular phosphoinositides, respectively. Whereas local levels of $PI(4,5)P_2$ can transiently drop when cells are stimulated with growth factors or hormones that activate PLC or phosphoinositide 3-kinases (PI3Ks), the total levels of $PI(4,5)P_2$ and PI(4)P remain remarkably constant. PI(4)P is >100-fold more abundant than PI(5)P in cells, and it is generally assumed that most $PI(4,5)P_2$ in mammalian cells is generated from PI(4)P via PIP5Ks (Balla, 2013). In B cell activation, transient recruitment of PIP5K1A is necessary for the generation of $PI(3,4,5)P_3$ for signal transduction (Saito et al., 2003).

Because PI(5)P constitutes ~1% of cellular phosphoinositides, it is uncertain whether this lipid contributes substantially to total cellular $PI(4,5)P_2$, raising speculation that the function of the PIP4Ks is primarily to decrease the level of PI(5)P (Jones et al., 2006; Wilcox and Hinchliffe, 2008). Recent work from our laboratory showed that the conversion of PI(5)P to $PI(4,5)P_2$ by PIP4K2A and PIP4K2B, likely on lysosomes, is critical to mediate the fusion between autophagosomes and lysosomes (Lundquist et al., 2018). This study argued that while the PIP4Ks generate only a small fraction of cellular $PI(4,5)P_2$, the location of the $PI(4,5)P_2$ generated by these enzymes plays an important role

This is an open access article under the CC BY-NC-ND license (http://creativecommons.org/licenses/by-nc-nd/4.0/).

in the completion of autophagy. There is also evidence for pools of PIP4K2A/PIP4K2B/PIP4K2C in the plasma membrane, Golgi, and nucleus, so the PIP4K enzymes are likely to have many other functions beyond autophagy regulation (Bultsma et al., 2010; Jones et al., 2006; Mackey et al., 2014).

PIP4K family members may also suppress insulin-PI3K-mammalian target of rapamycin complex 1 (mTORC1) signaling *in vivo*, despite their enzymatic function to synthesize PI(4,5)P_2. Homozygous germline deletion of *Pip4k2b*$^{-/-}$ in mice causes reduced adiposity and increased insulin sensitivity in muscle (Lamia et al., 2004), and *Pip4k2c*$^{-/-}$ mice have enhanced TORC1 signaling (Shim et al., 2016). In addition, the accumulation of PI(5)P, resulting from the loss of the highly active forms of PIP4K, increases signaling through the PI3K pathway (Carricaburu et al., 2003; Pendaries et al., 2006). While this is one mechanism by which PIP4Ks could influence PI3K activity, additional possibilities remain to be explored. For example, it was previously shown that overexpressed PIP4K2A can interact with all three PIP5K isoforms, but the nature of this binding remains a mystery (Hinchliffe et al., 2002), Overall, it is not clear how membrane lipid changes underlie the molecular mechanism by which the PIP4Ks regulate the PI3K pathway, and it is unknown whether one PIP4K isoform can compensate for others to suppress growth factor signal transduction.

In this study, we demonstrate that PIP4Ks have distinct catalytic and non-catalytic functions in controlling cellular metabolism and that it is the loss of catalytic-independent functions of PIP4Ks that underlie enhanced insulin signaling. We report our findings in parallel with an independent study in *Drosphila*, placing PIP4K as an evolutionarily conserved modulator of the PI3K pathway (Sharma et al., 2019).

RESULTS

Loss of PIP4K Family Members Does Not Affect Cell Viability

To investigate the role of PIP4K enzymes in cellular signaling, we generated tools to systematically deplete individual members of the PIP4K family. We cloned a series of lentiviral-based tandem miR-E-based short hairpin RNAs (shRNAs) (Tables S1 and S2) and induced the stable knockdown of PIP4K family isoforms in HeLa cells and other human immortalized or transformed cells (Figures 1A, S1A–S1C, and S2A–S2E; Fellmann et al., 2011, 2013; Pelossof et al., 2017). shRNA-mediated silencing of one or all of the PIP4Ks did not result in gross changes in morphology or cause a major change in the growth rate of the cells examined (Figure S1D). As an orthogonal approach, we used CRISPR/Cas9 to delete *PIP4K2A, PIP4K2B*, and *PIP4K2C* in HEK293T cells (Figure 1B; Tables S1 and S2), with similar results (Ran et al., 2013).

Loss of PIP4Ks Results in Increased PI(5)P levels, Increased PI3K Activation, and Defects in Autophagy

PIP4K2A/B/C triple knockout 293T cells (hereafter TKO) and triple knockdown HeLa cells (hereafter TKD) recapitulated previously reported phenotypes in which PIP4K enzymes were depleted. As reported (Gupta et al., 2013), the loss of all three enzymes conferred a 2-fold increase in their substrate, PI(5)P (Figures 1C and 1D). In addition, TKD cells exhibited increased PI3K signaling upon insulin stimulation (Figure 1E), which is consistent with observations of increased insulin sensitivity in *Pip4k2b*$^{-/-}$ mice (Carricaburu et al., 2003; Lamia et al., 2004). Furthermore, 293T TKO cells accumulated LAMP1 lysosomes, which we attributed to defects in autophagosome-lysosome fusion as described in *Pip4k2a*$^{-/-}$, *Pip4k2b*$^{-/-}$mouse embryonic fibroblasts (MEFs) (Figure 1F; Lundquist et al., 2018).

Cellular PI(4,5)P_2 Is Increased upon Depletion of PIP4K

Depletion of the three PIP4Ks in cells altered the levels of phosphoinositides beyond PI(5)P. In both TKD and TKO cells, we observed a surprising increase in PI(4,5)P_2 and concomitant decrease in PI(4)P (Figures 1G–1J and S2F–S2P). Basal levels of PI(3,4,5)P_3 during growth in culture are typically below the detection limit in high-performance liquid chromatography (HPLC)-based assays. However, we were able to detect the basal elevation of PI(3,4,5)P_3 in TKO cells, suggesting that the increased PI(4,5)P_2 is able to be used by PI3K (Figure 1K). PI(4,5)P_2 constitutes ~50% of all phosphoinositides, although the majority is bound to the cytoskeletal and scaffolding proteins required for cell structure, migration, and adhesion (Brown, 2015; Choi et al., 2015). While PI(4,5)P_2 is highly abundant, local production of PI(4,5)P_2 by PIP5Ks offers spatiotemporal control of signaling through the PI3K and PLC pathways (Choi et al., 2015; Saito et al., 2003; Xie et al., 2009).

Identification of a Catalytic-Independent Function of PIP4K

Members of the PIP4K family have dramatically different catalytic rates. For instance, PIP4Kα (*PIP4K2A*) has 1,000-fold higher activity than PIP4Kγ (*PIP4K2C*), which is considered near-enzymatically dead (Clarke and Irvine, 2013). Analysis of PI(4,5)P_2 levels in cells with single or double knockdown of PIP4K isoforms revealed an additive effect among all three isoforms that does not correlate with their relative catalytic activities (Figures 2A and 2B). Double knockdown of the most active isoforms, PIP4Kα/β, did not phenocopy the triple knockdown, suggesting that catalytic activity is not the most important factor in regulating PI(4,5)P_2 levels. To evaluate whether the catalytic activity of PIP4K enzymes is important for PI(4,5)P_2 regulation, we generated shRNA-resistant hemagglutinin (HA)-tagged kinase-active or kinase-dead PIP4K isoforms (Figures 2C and 2D).

The expression of either kinase-active or kinase-dead (PIP4K2A^{KD}) PIP4Ks rescued PI(4,5)P_2 levels (Figures 2E and 2F). Moreover, PI(4)P levels also returned to baseline with the expression of either kinase-active or kinase-dead PIP4K2A in both TKD and TKO cell lines (Figures 2G and 2H). In contrast, only the active PIP4K2A restored normal PI(5)P levels, indicating that the elevation of this lipid species in knockdown cells, in contrast to PI(4,5)P_2, is due to the loss of PIP4K enzymatic activity (Figures 2I and 2J). We used a 3′ internal ribosome entry site (IRES)-GFP tag to sort for cell populations with low and high expression of PIP4K2A^{KD} populations, PIP4K2A^{KD_low} and PIP4K2A^{KD_high}, respectively (Figure S3A). HPLC analysis of these cell lines shows a dose-dependent decrease in PI(4,5)P_2 and increase in PI(4)P correlated with the levels of PIP4K2A^{KD} expression (Figures S3B and S3C). Thus, we conclude that PIP4Ks have

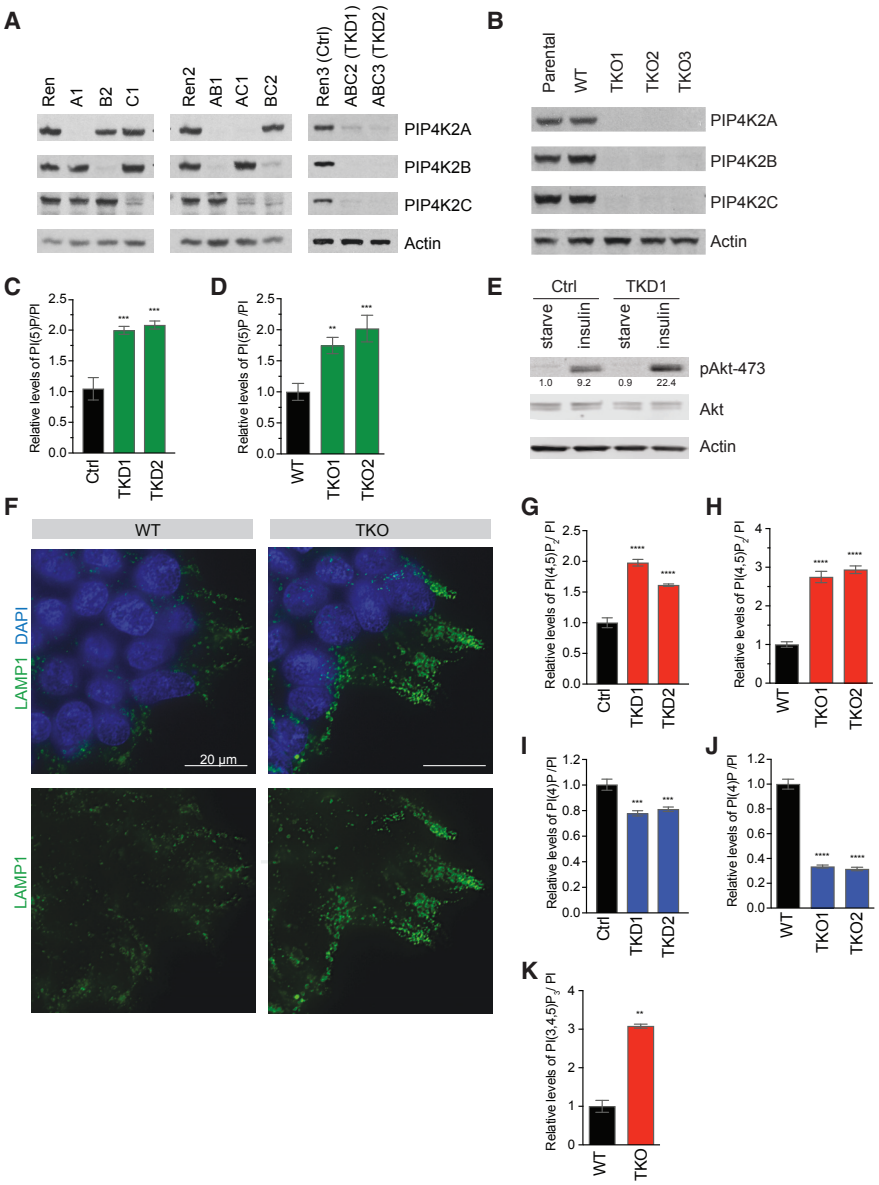

Figure 1. Validation of Tools to Eliminate All Three PIP4K Isoforms Reveals Paradoxical Increase in PI(4,5)P_2

(A) Western blots showing the efficiency of knockdown of PIP4K isoforms in HeLa cells. Cell line notation and their descriptions are listed in Table S2.

(B) Western blots showing 293T clones with CRISPR-mediated knockout of *PIP4K2A, PIP4K2B*, and *PIP4K2C,* with cell line descriptions in Table S2. Parental cell line is in the first lane, and the CRISPR clonal cell line with intact PIP4K is designed as WT. A faint non-specific band that runs slightly faster than PIP4Ks is just visible.

(C and D) Quantification by HPLC of PI(5)P, which increases in cells with the loss of PIP4K, shown in HeLa TKD cells (C) as well as 293T TKO cells (D).

(E) Knock down of PIP4K enhances insulin signaling in HeLa cells, as shown by western blot. Quantification by Li-Cor indicated the respective bands below.

(F) Immunofluorescence detection of lysosomal marker Lamp1 showing increased lysosomal accumulation in 293T TKO versus control cells. Representative images shown.

(G and H) PI(4,5)P_2 increases in cells with loss of PIP4K, shown in HeLa TKD cells (G) and 293T TKO cells (H), measured by HPLC.

(I and J) PI(4)P decreases in cells with loss of PIP4K, shown in HeLa TKD cells (I) and 293T TKO cells (J), measured by HPLC.

(K) 293T TKO cells have higher levels of PI(3,4,5)P_3, as measured by HPLC.

Significance calculated using ANOVA with Holm-Sidak multiple comparisons to control cell line with intact PIP4K. $^{**}p < 0.01$, $^{***}p < 0.001$, and $^{****}p < 0.0001$. Data are represented as means ± SEMs. n = 3.

a catalytic-independent role in maintaining the homeostasis of cellular PI(4)P and PI(4,5)P_2 levels, distinct from their enzymatic function in converting PI(5)P to PI(4,5)P_2.

PIP5K Activity Is Elevated in Cells Depleted of PIP4K

The observed increase in PI(4,5)P_2 relative to PI(4)P is consistent with a robust production of PI(4,5)P_2 by the PIP5Ks. We

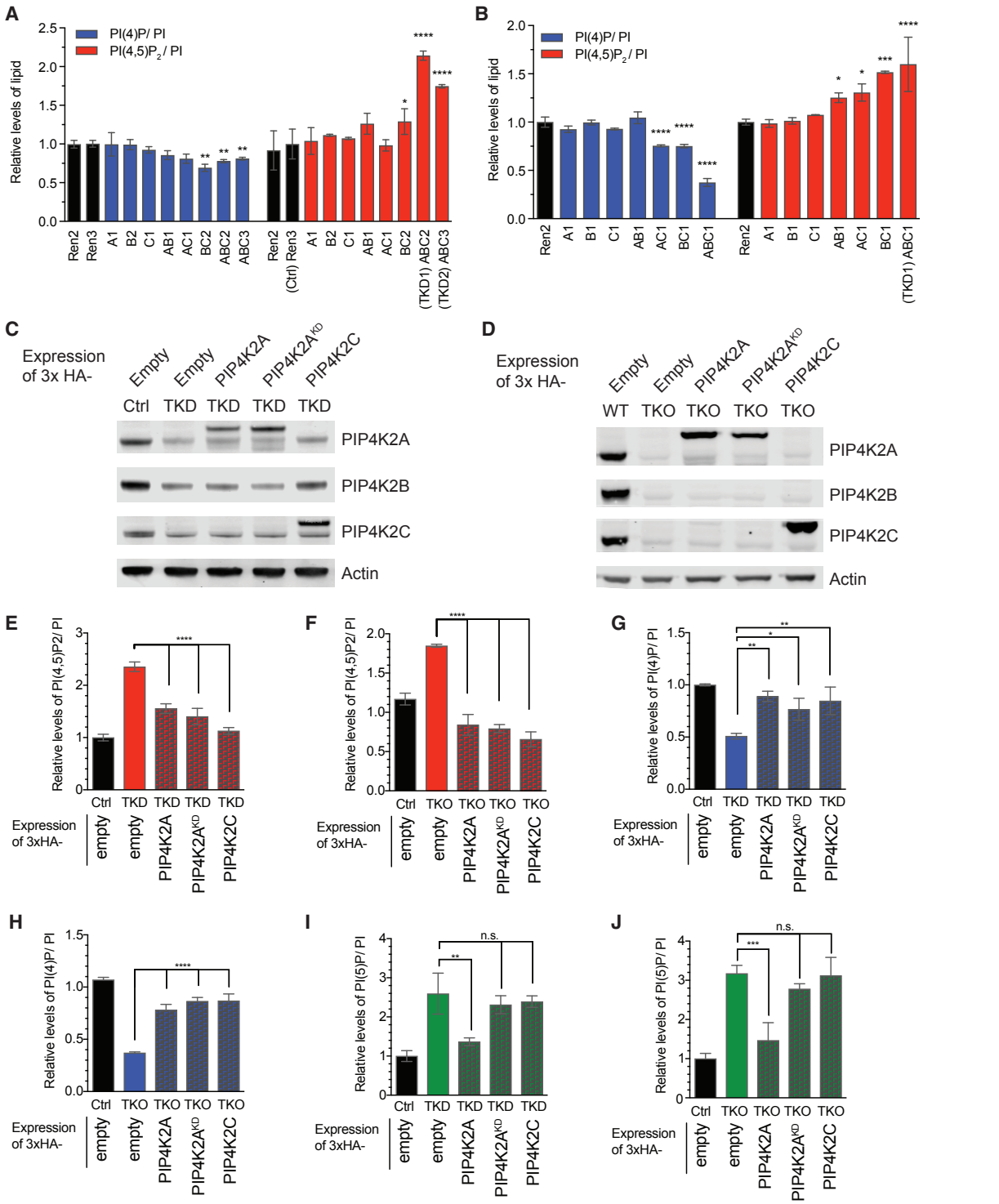

Figure 2. Identification of a Catalytic-Independent Function of PIP4K

(A and B) Quantification of PI(4)P and PI(4,5)P_2 levels by HPLC upon knockdown of one or multiple isoforms of PIP4K in 293T cells (A) or HeLa cells (B) using tandem shRNA constructs. Hairpin constructs are indicated on the x axis, with descriptions in Table S2.

(C and D) Western blot validation of rescue cell line panel with reconstitution of kinase-active or kinase-dead PIP4K2A^{KD} or kinase-active PIP4K2C into HeLa TKD cells (C) or 293T TKO cells (D) at near-endogenous levels. Tagged 3xHA-PIP4K proteins are larger than the endogenous protein. A faint non-specific band is visible running slightly faster than the endogenous protein.

(legend continued on next page)

measured PIP5K activity in mechanically disrupted cells and found that TKO cells exhibit elevated PIP5K activity, which is consistent with the model that PIP5K is more active in the absence of PIP4K. The increased PIP5K activity was reversed in cells expressing either kinase-active or kinase-dead PIP4K isoforms, indicating that it is not dependent on the enzymatic activity of these proteins (Figure 3A).

All three isoforms of PIP5K are stimulated by phosphatidic acid (PA) and by association with G-proteins such as Rac (Jenkins et al., 1994; Weernink et al., 2004). However, PIP5K activation in PIP4K-depleted cells is not due to these upstream effectors, as cells with PIP4K knockdown did not exhibit increased PA levels (Figure S3D), and the knockout of Rac1 did not abrogate the ability of PIP4K to modulate levels of PI(4)P and PI(4,5)P_2 (Figures S3E–S3G). Furthermore, protein levels of PIP5K1A and PIP5K1C were not consistently altered in response to knockdown or knockout of the PIP4K family (Figures S3H and S3I).

Lastly, we considered the possibility that PIP4K has a catalytic-independent role in masking PI(5)P, thereby reducing the availability of adaptor proteins that may inhibit PIP5K activity. To test whether the increased availability of PI(5)P can enhance PIP5K activity to decrease the PI(4)P to PI(4,5)P2 ratio, we transfected cells with Ipgd, a bacterial 4-phosphatase recognizing PI(4,5)P_2. While transfection of Ipgd into 293T cells caused a dramatic increase in cellular PI(5)P, HPLC analysis of cellular phosphoinositides did not suggest a concomitant increase in PIP5K activity. The increased availability of PI(5)P in cells with intact PIP4K (wild type [WT]) did not cause a decreased ratio of PI(4)P to PI(4,5)P_2. In addition, the introduction of Ipgd into TKO cells caused a large increase in PI(5)P, but it did not change the measured PI(4)P or PI(4,5)P_2 levels (Figures S3J–S3L). These results suggest that the availability of PI(5)P does not mediate the observed change in PIP5K activity.

PIP4K Can Inhibit PIP5K through Direct Interactions on the Surface of Negatively Charged Membranes

Members of the PIP4K and PIP5K family have been reported to physically interact (Hinchliffe et al., 2002; Huttlin et al., 2017). Such an interaction would be an opportunity for PIP4K to directly inhibit PIP5K. Notably, PIP4K family members are considerably more abundant than PIP5K family members, making the stoichiometric ratio favorable for PIP4Ks to inhibit PIP5Ks (Itzhak et al., 2016; Wiśniewski et al., 2014). To test whether the altered PIP5K activity in PIP4K-depleted cells could be a result of a disrupted physical interaction between these two kinase families, we measured *in vitro* kinase activity with purified proteins. We found that all three PIP4K isoforms could directly inhibit the PIP5K2A-catalyzed phosphorylation of PI(4)P into PI(4,5)P_2 (Figure 3B). To eliminate the possibility that a small molecule contaminant from our PIP4K purifications could inhibit PIP5K1A, we boiled PIP4K2C and found that denatured PIP4K2C could no longer inhibit PIP5K1A (Figure 3C). To investigate whether the interactions between PIP4K and PIP5K occur at the membrane bilayer, we repeated the experiment with detergent to eliminate the formation of PI(4)P liposomes. Presenting phosphoinositides in Triton X-100 micelles enhances the activity of some PI kinases, such as the PI4Ks (Guo et al., 2003), but we found that it reduced PIP5K1A activity overall. The addition of detergent eliminated the ability of PIP4K2A to inhibit PIP5K1A (Figure 3D). These data suggest that recruitment of both proteins to the membrane surface is required to mediate the inhibitory interaction. As we performed this assay using vast molar excess of the substrate PI(4)P relative to the levels of both enzymes, we postulate that sequestration of PI(4)P by PIP4Ks is unlikely to account for this inhibition. As expected, given the membrane-dependence of PIP4K and PIP5K association, attempts to co-immunoprecipitate PIP4K with PIP5K in the presence of detergent were unsuccessful. However, by chemical crosslinking in intact cells, we demonstrated the interaction of 3xHA-tagged PIP5K1A expressed at near-endogenous levels with endogenous PIP4K2A (Figures 3E and 3F). Furthermore, glutathione S-transferase (GST)-PIP4K2C-conjugated glutathione beads pulled down the majority of PIP5K1A in 293T lysates, but only a tiny fraction of PIP5K1C (Figures 3G and 3H), supporting the hypothesis that PIP4Ks interact with PIP5K1A in cells to regulate PI(4,5)P_2 levels.

To further define the nature of this interaction, we generated PIP4K2C variants and assessed their ability to inhibit PIP5K1A activity *in vitro*. Human PIP4K2A (PDB: 2YBX) and PIP4K2C (PDB: 2GK9) have been crystallized, while the only PIP5K family member that has been crystallized is from *Danio rerio*, and it forms a crystal structure similar to that of the PIP4K proteins (PDB: 5E3S) (Muftuoglu et al., 2016). PIP4K2C crystallizes as a tetramer via side-by-side interactions of two dimers in which all four catalytic pockets appear on the same side of the positively charged tetramer. Thus, we focused our mutagenesis efforts on PIP4K2C, beginning with a truncation mutant from the COSMIC database carrying a frameshift mutation after amino acid (aa) 132 of PIP4K2C (https://cancer.sanger.ac.uk/cosmic). This truncated mutant, which maintains the residues involved in both dimeric interactions and tetrameric interactions was as potent as full-length PIP4K2C in its ability to inhibit PIP5K1A activity *in vitro* (Figure S4A). Hence, we explored the first 132 residues of PIP4K2C and identified 2 regions that face the opposing dimer in the tetrameric structure: aas 69–75 (VMLLPDD) and aas 89–95 (FHRENLP) (Figures 3I and S4B). Mutating 74DD → NN or 91REN → EED of GST-PIP4K2C did not prevent this protein from inhibiting PIP5K1A (Figure S4C). However, introducing mutations into this region that are likely to impair both hydrophobic and charge interactions across the dimer-dimer interaction (VMLLPDD → EIFLPNN), hereafter called PIP4K2C^{VD}, resulted in a loss of interaction with PIP5K1A (Figure 3J). Furthermore, PIP4K2C^{VD} failed to inhibit PIP5K1A activity (Figure 3K) while maintaining PIP4K activity (Figures S4D and S4E), confirming that the protein is folded and functional. To confirm that this interaction between PIP4Ks and PIP5K1A is the physiologic mechanism of increased PI(4,5)P_2 production observed in our

(E–J) Quantification by HPLC of PI(4,5)P_2 in HeLa TKD rescue cell lines (E) and 293T TKO rescue cell lines (F). Quantification of PI(4)P in HeLa TKD rescue cell lines (G) and 293T TKO rescue cell lines (H). Quantification of PI(5)P in HeLa TKD rescue cell lines (I) and 293T TKO rescue cell lines (J).
Significance calculated using ANOVA with Holm-Sidak multiple comparisons to TKD or TKO cell lines. *$p < 0.05$, **$p < 0.01$, ***$p < 0.001$, and ****$p < 0.0001$. Data are represented as means ± SEMs. n = 3.

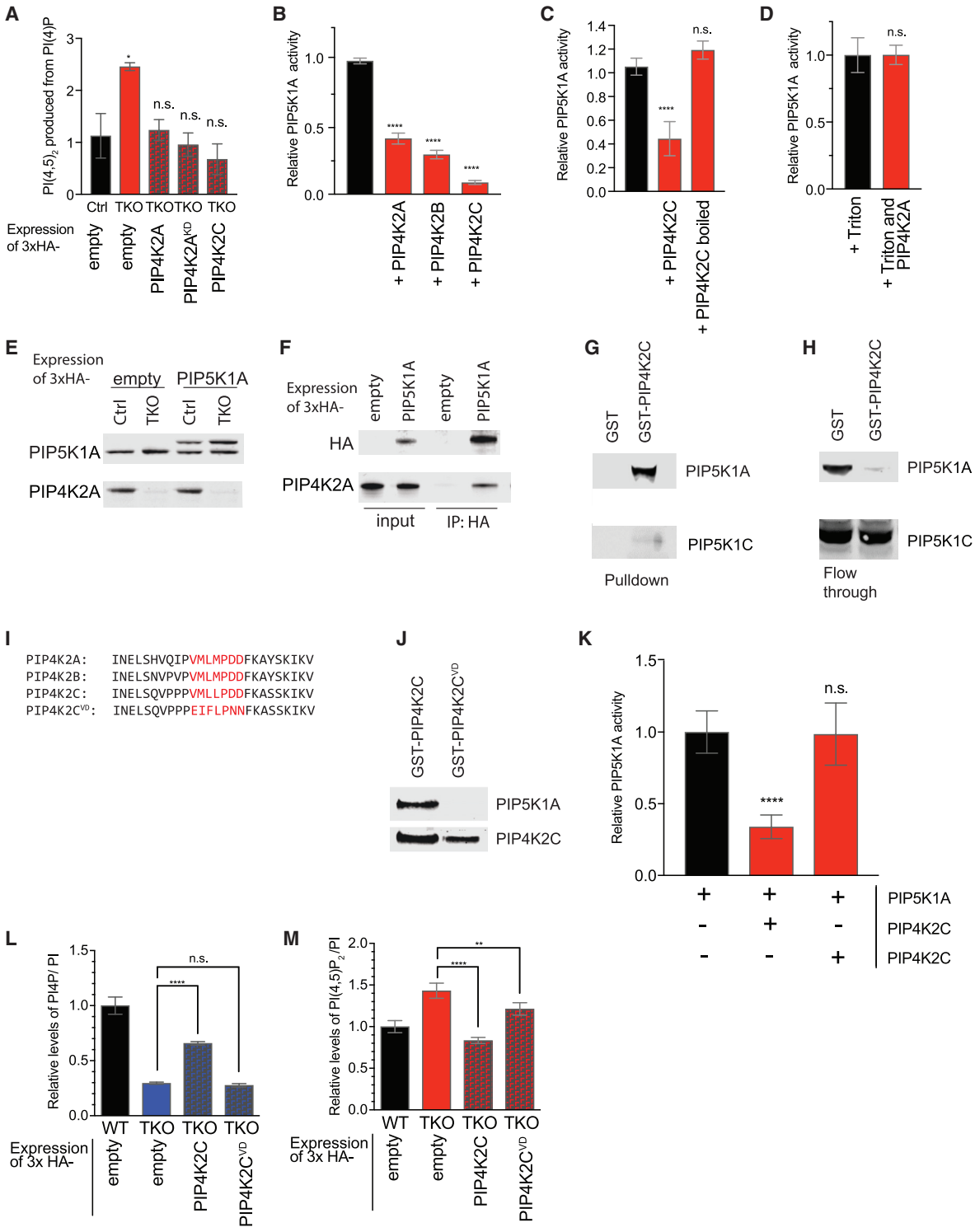

Figure 3. PIP4K Inhibits PIP5K Activity

(A) Changes in PIP5K activity in 293T cells. Cell pellets were normalized to cell number and sonicated in the presence of excess PI(4)P. Radioactive ATP^{32} was added for kinase reaction. Lipids were extracted and quantified by TLC, with confirmation by HPLC after deacylation.

(B–D) Quantification of *in vitro* kinase assay measuring conversion of PI(4)P to radiolabeled PI(4,5)P_2 by PIP5K1A. PIP5K1A activity is inhibited *in vitro* by addition of 2- to 10-fold molar excess of PIP4K2A, PIP4K2B, or PIP4K2C (B). Once denatured, PIP4K2C no longer inhibits PIP5K1A (C). In the presence of 0.1% Triton X-100, PIP4K2A no longer inhibits PIP5K1A activity (D).

(legend continued on next page)

CRISPR knockout cells, we reconstituted the TKO cells with PIP4K2C^{VD} or WT PIP4K2C, as previously described (Figure S4F). Notably, the PIP4K2C^{VD} mutant failed to reverse the decreased PI(4)P and increased PI(4,5)P_2 observed in the TKO cells (Figures 3L and 3M), which is consistent with a failure to interact with or inhibit PIP5K1A, as we had observed *in vitro*.

These results reveal a mechanism for the regulation of PI(4,5)P_2 production, whereby PIP5K1A is negatively regulated by a direct interaction with the N-terminal motif VMLΦPDD of PIP4Ks. We propose that a fraction of cellular PIP4Ks directly interact with PIP5K enzymes at membranes enriched in PI(4)P and function to attenuate the PIP5K-mediated conversion of PI(4)P to PI(4,5)P_2. Although historically, attempts to directly visualize the subcellular localization of PIP4Ks have been inconsistent, recent global quantitative mapping of protein subcellular localization suggests that both PIP5Ks and PIP4Ks are largely bound to plasma membranes (Bultsma et al., 2010; Hinchliffe et al., 1999, 2002; Itoh et al., 1998; Itzhak et al., 2016; Kunz et al., 2000).

Structural Role of PIP4K in Regulating PIP5K and PI3K Pathway Is Distinct from Its Catalytic Role in Autophagy

Levels of PI(4,5)P_2 are remarkably stable to perturbations of its precursor PI(4)P (Nakatsu et al., 2012), yet we find that depletion of the PIP4K family members results in nearly 2-fold changes in PI(4)P and PI(4,5)P_2 (Figures 1G–1J). Insulin activation of the PI3K pathway is initiated at the plasma membrane, where conversion of PI(4,5)P_2 into PI(3,4,5)P_3 recruits effector proteins Akt and Pdk1 to propagate signaling cascades. We hypothesized that, in PIP4K-depleted cells, increased PI(3,4,5)P_3 may be attributed to the activation of the PI3K pathway due to elevated production of its substrate, PI(4,5)P_2. During acute stimulation, local production of PI(4,5)P_2 by PIP5K1A sustains the activation of the PI3K pathway in B cells, keratinocytes, and breast adenocarcinoma (Choi et al., 2016; Saito et al., 2003; Xie et al., 2009). HPLC analysis of lipids showed that PIP4K knockout cells exhibited a 4-fold increase in PI(3,4,5)P_3 upon acute insulin stimulation (Figure 4A). Consistent with the model that PIP4Ks suppress insulin signaling by their catalytic-independent suppression of PI(4,5)P_2 synthesis by the PIP5Ks, expression of the kinase-dead PIP4K2A or the near-kinase-dead PIP4K2C in TKO cells was able to reverse the insulin-dependent increase in PI(3,4,5)P_3 accumulation. Expression of the PIP4K2C^{VD} mutant failed to rescue PI(3,4,5)P3 levels (Figure 4A), which is consistent with our model that the VMLΦPDD motif mediates negative regulation of the PI3K pathway.

Furthermore, HeLa TKD cells displayed enhanced PI3K pathway activation, as judged by S473 phosphorylation of AKT as well as AKT-mediated phosphorylation of PRAS40 (Manning and Toker, 2017; Figures 4B and 4C). Expression of either PIP4K2A^{KD} or PIP4K2C reversed the enhanced insulin sensitivity, whether measured by PI(3,4,5)P_3 levels or AKT activation. Our results indicate that increasing PIP5K activity by eliminating PIP4K isoforms drives the overproduction of PI(4,5)P_2 in plasma membrane pools that may be used by PI3K during insulin signaling.

Finally, we asked whether the non-catalytic function of PIP4Ks was required for the previously reported role of PIP4K2A in mediating autophagy (Lundquist et al., 2018). As expected, loss of PIP4Ks resulted in the accumulation of LAMP1^{+} lysosomes and increased transcription factor EB (TFEB) transcriptional targets. However, unlike the changes observed in phosphoinositides, only reconstitution with kinase-active but not kinase-dead PIP4K2A showed restored regulation of autophagy (Figure 4D–4F). This work highlights the complexity and multi-functionality of PIP4K enzymes.

DISCUSSION

In this study, we show that the proteins encoded by the *PIP4K2A, PIP4K2B*, and *PIP4K2C* genes have distinct catalytic and non-catalytic functions and provide insight into the phenotypes observed in Pip4k-deficient mice. The roles of the PIP4K2A and PIP4K2B isoforms in autophagosome-lysosome fusion that were recently reported in MEFs and *in vivo* using mice with targeted liver-specific PIP4K deletions (Lundquist et al., 2018) depend on the ability of these enzymes to convert PI(5)P to PI(4,5)P_2. However, our present study revealed that the increased insulin sensitivity previously observed in *Pip4k2b*$^{-/-}$ mice (Lamia et al., 2004) is due to the loss of a non-catalytic function of PIP4K2B in suppressing the ability of PIP5Ks to produce PI(4,5)P_2 to be used as the substrate for PI 3-kinase. One confounding issue could be the increase in PI(5)P observed when PIP4Ks are depleted. Previous studies characterizing Ipgd, a bacterial 4-phosphatase of PI(4,5)P_2, have demonstrated that increasing PI(5)P levels prolongs Akt signaling (Carricaburu et al., 2003; Niebuhr et al., 2002; Pendaries et al., 2006). The model presented by Carricaburu et al. (2003) describes how increased cellular PI(5)P inhibits PI(3,4,5)P_3 -specific

(E) Western blot validation of near-endogenous level expression of 3xHA-PIP5K1A levels in 293T control and TKO cells. Tagged 3xHA-PIP5K1A is slightly larger than the endogenous protein.

(F) Pull-down using anti-HA beads from 293T WT cells expressing empty 3xHA vector (empty) or 3xHA-PIP5K1A (PIP5K1A). Western blot of input (first two lanes) and immunoprecipitation of endogenous PIP4K2A with PIP5K1A (second two lanes).

(G and H) 293T lysates were incubated with beads pre-incubated with either GST or GST-PIP4K2C, used as bait. Pull-downs analyzed by western blot strongly to detect the enrichment of PIP5K1A and PIP5K1C (G). Analysis of flow-through reflects the extent to which lysate is depleted of PIP5K1A and PIP5K1C by bait (H).

(I) Sequence homology of N-terminal region in PIP4K. Mutated residues of PIP4K2C aa69–75 are indicated in red.

(J) 293T lysates were incubated with beads conjugated to GST-PIP4K2C or GST-PIP4K2C^{VD}, used as bait. Bead pull-downs were analyzed by western blot for the presence of PIP5K1A, which is able to bind WT PIP4K2C but not PIP4K2C^{VD}.

(K) Quantification of *in vitro* kinase assay measuring the conversion of PI(4)P to radiolabeled PI(4,5)P_2 by PIP5K1A, which is inhibited by PIP4K2C but not PIP4K2C^{VD}.

(L and M) Quantification by HPLC of PI(4)P (L) and PI(4,5)P_2 (M) in HEK293T TKO cell lines rescued with PIP4K2C and PIP4K2C^{VD}.

Significance calculated using ANOVA with Holm-Sidak multiple comparisons to control cell line. **$p < 0.01$, ****$p < 0.0001$, and n.s., not significant. Data are represented as means ± SEMs. n = 3.

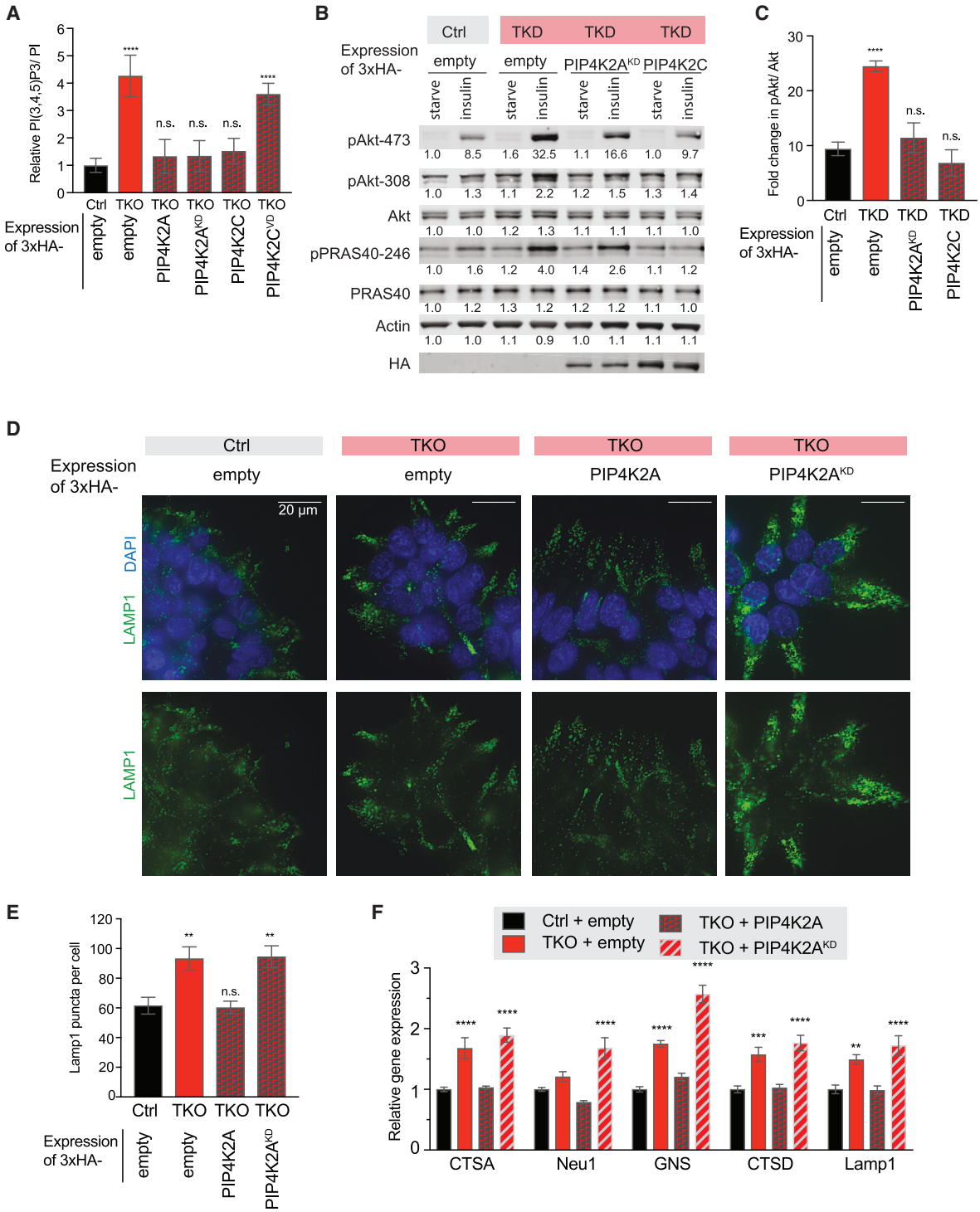

Figure 4. Structural Role of PIP4K in Regulating PIP5K and the PI3K Pathway Is Distinct from Its Catalytic Role in Autophagy

(A) Insulin stimulation of PI(3,4,5)P_3 synthesis by PI3K in 293T rescue cell lines, quantified by HPLC. Cells were serum starved for 20 h, then stimulated with 50 ng/mL insulin for 5 min.

(B) Insulin stimulation of Akt activation in HeLa rescue cell line panel. Cells were serum starved for 12 h, then stimulated with 250 ng/mL insulin for 10 min. Western blot band intensities were measured by Li-Cor and are indicated under the relevant band.

(C) Quantification of insulin-stimulated increase in pAkt-473in HeLa rescue cell line panel, normalized to total Akt. n = 3.

(legend continued on next page)

phosphatase, thereby leading to an increase in $PI(3,4,5)P_3$ levels. This suggests that in certain settings, the catalytic activity of PIP4K modulates Akt signaling through the control of PI(5)P levels. However, our data show that reconstitution with kinase-dead PIP4K fully rescues $PI(3,4,5)P_3$ levels and Akt phosphorylation in response to insulin signaling, despite not reducing PI(5)P, arguing that the model proposed above cannot account for our observations.

We show that PIP4Ks and PIP5Ks directly interact and that mutating five conserved aas of PIP4K2C can abrogate this interaction and prevent PIP5K suppression. A role in regulating PIP5K activity may explain why PIP4Ks are highly abundant in cells, in excess of PIP5Ks, which are thought to produce most of the $PI(4,5)P_2$. Because both PIP4Ks and PIP5Ks are bound to negatively charged membranes, these enzymes could also alter local membrane structures or recruit other enzymes to modify PIP5Ks to further modulate their activities. Future studies will address these possibilities.

Our results indicate that the design of drugs to promote the degradation of PIP4Ks may mitigate insulin resistance and possibly retard the progression of type 2 diabetes. Recently emerging technologies raise the possibility that one could degrade specific PIP4K proteins by linking them to E3 ligases (Bondeson and Crews, 2017). We initially had reservations about the development of such drugs due to the embryonic lethality of germline co-deletion of PIP4K2B and PIP4K2C or PIP4K2A and PIP4K 2B (Emerling et al., 2013; Shim et al., 2016). In addition, Emerling et al. (2013) and Lundquist et al. (2018) reported the reduced viability of MEFs upon the loss of PIP4K2A and/or PIP4K2B in cell lines with deficient p53 signaling. However, our results in a panel of cancer lines suggest that most cell lines do not require PIP4K isoforms for viability when grown in tissue culture with full nutrients (Figure S2). Embryonic lethality from the co-deletion of murine PIP4K isoforms may be attributed to the developmental defects required for mammalian development or nutrient stress in the perinatal period (Emerling et al., 2013; Shim et al., 2016), and partial and/or tissue-specific targeted depletion may be well tolerated.

We note that each tissue has a different ratio of PIP4K2A: PIP4K2B:PIP4K2C, and therefore it remains to be seen whether targeting a subset of the PIP4K family in humans will enhance systemic insulin sensitivity. The PIP4K2B knockout mice exhibit increased insulin sensitivity that is not seen in PIP4K2A and PIP4K2C knockout mice. This is likely because PIP4K2B is the predominant isoform in skeletal muscle, a primary site of insulin-mediated glucose uptake. It will be interesting to see whether other insulin-responsive tissues, such as liver and adipose tissue, will become sensitized to insulin if multiple PIP4K isoforms are depleted.

PIP4K family members repress the conversion of PI(4)P to $PI(4,5)P_2$ and subsequently to $PI(3,4,5)P_3$ to limit PI3K pathway signaling. This occurs by a mechanism that does not require the catalytic activity of these enzymes, while they directly catalyze the conversion of PI(5)P to $PI(4,5)P_2$ to promote autophagy. How did these two disparate functions come to reside in the same protein? One possibility is to ensure that the levels of PI(4)P remain high at local sites of autophagosome-lysosome fusion. Several recent studies indicate that PI(4)P is required for autophagosome-lysosome fusion and that in some cases this PI(4)P is derived from an inositol 5-phosphatase acting on local pools of $PI(4,5)P_2$ (De Leo et al., 2016; Wang et al., 2015). Thus, the PIP4Ks may be both producing the local $PI(4,5)P_2$ at the autophagosome-lysosome junction and ensuring that upon conversion to PI(4)P, it is not converted back to $PI(4,5)P_2$ by a PIP5K. This model would ensure a unidirectional conversion of PI(5)P to PI(4)P and efficient autophagosome-lysosome fusion. The partial localization of PIP4K2C to the Golgi (Clarke et al., 2008) could also suppress the conversion of Golgi PI(4)P to $PI(4,5)P_2$ to maintain the high local concentration of the PI(4)P that is needed for vesicle trafficking at this location.

Given the global increase in $PI(4,5)P_2$ observed, there are undoubtedly multiple $PI(4,5)P_2$ mediated functions that will be affected. It will be interesting to characterize how the accumulation of $PI(4,5)P_2$ in PIP4K-depleted cells affects cellular processes beyond growth factor signaling, such as cell adhesion, migration, and/or calcium signaling. Furthermore, it will be essential to examine how this change affects the localization and levels of other phosphoinositides within cells.

Our findings highlight an unexpected and important separation of catalytic and non-catalytic functions in PIP4K family enzymes and indicate new avenues for intervention in enhancing insulin signaling.

STAR★METHODS

Detailed methods are provided in the online version of this paper and include the following:

- KEY RESOURCES TABLE
- CONTACT FOR REAGENT AND RESOURCE SHARING
- EXPERIMENTAL MODEL AND SUBJECT DETAILS
  - Cell lines, authentication
- METHOD DETAILS
  - Cell lysis and immunoblotting
  - Generation of lentivirus, viral transduction
  - Generation of cell lines with CRISPR knockout of PIP4K
  - Generation of cell lines with miR-E knockdown of PIP4K
  - Generation of mammalian and bacterial expression vectors
  - Measurement of phosphoinositides with high performance liquid chromatography
  - Measurement of phosphatidic acid using LCMS

(D and E) Immunofluorescence detection of lysosomal marker Lamp1 in the 293T rescue cell line panel shows dependence on catalytic activity to rescue increased lysosomal accumulation. Representative images are shown (D), and full quantification is detailed (E).

(F) Quantification of TFEB target gene expression by qRT-PCR in 293T rescue cell line panel.

Significance calculated using ANOVA with Holm-Sidak multiple comparisons to control cell line. *$p < 0.05$, **$p < 0.01$, ***$p < 0.001$, ****$p < 0.0001$, and n.s., not significant.

- Immunoprecipitation
- Protein Purification
- In-vitro kinase assays
- GST Pulldown assays
- Fluorescence microscopy
- qRT-PCR

● QUANTIFIICATION AND STATISTICAL ANALYSIS

SUPPLEMENTAL INFORMATION

Supplemental Information can be found online at https://doi.org/10.1016/j.celrep.2019.04.070.

ACKNOWLEDGMENTS

We thank all of the members of the Cantley laboratory for feedback. We thank Jared Johnson for chemistry and biochemistry consultations. We thank Yuxiang Zheng for sharing expertise on the HPLC analysis of phosphoinositides. We thank Hyeseok Shim for insight on PIP4K2C biology. This work was supported by grants from the NIH (R35 CA197588 and U54 U54CA210184) and the Lustgarten Foundation and by grants to J.M.B., including the NIH Pathway to Independence (R00 GM110121), the National Science Foundation (NSF) CAREER (CHE-1749919), and the Beckman Young Investigator (Arnold and Mabel Beckman Foundation) to L.C.C. L.E.D. was supported by a K22 Career Development Award from the National Cancer Institute (NCI)/NIH (CA 181280-01). D.G.W. was supported by a Medical Scientist Training Program grant from the NIH (T32GM007739) to the Weill Cornell/Rockefeller/Sloan Kettering Tri-Institutional MD-PhD Program, and T.W.B. was supported by an NSF graduate research fellowship (DGE-1650441). This research was funded in part by Petra Pharmaceuticals. Cell sorting was partially supported by an NIH S10 award (1S10 OD019986-01). The laboratory of L.C.C. also receives funding from Petra Pharmaceuticals for research on phosphoinositide kinases.

AUTHOR CONTRIBUTIONS

D.G.W., M.N.P., L.E.D., and L.C.C. formulated the research plan and interpreted the experimental results. D.G.W., M.N.P., and M.R.L. designed and performed the experiments with assistance from J.Y.S., O.M., S.A., A.H., and M.F. L.E.D., B.D.H., T.W.B., J.M.B., and T.J.Y. provided the reagents and helped interpret the experimental results. D.G.W., M.N.P., and L.C.C. wrote the manuscript, and all of the authors edited it.

DECLARATION OF INTERESTS

L.C.C. is a founder and member of the SAB and holds equity in Agios Pharmaceuticals and Petra Pharmaceuticals, companies developing drugs for treating cancer. L.E.D. is a consultant and an advisory board member for Mirimus, which has licensed some of the shRNA technology used in this study. The laboratory of L.C.C. holds patents on targeting phosphoinositide kinases for cancers and insulin resistance.

Received: September 6, 2018
Revised: February 6, 2019
Accepted: April 16, 2019
Published: May 14, 2019

REFERENCES

Balla, T. (2013). Phosphoinositides: tiny lipids with giant impact on cell regulation. Physiol. Rev. *93*, 1019–1137.

Bondeson, D.P., and Crews, C.M. (2017). Targeted Protein Degradation by Small Molecules. Annu. Rev. Pharmacol. Toxicol. *57*, 107–123.

Brown, D.A. (2015). PIP2Clustering: from model membranes to cells. Chem. Phys. Lipids *192*, 33–40.

Bultsma, Y., Keune, W.J., and Divecha, N. (2010). PIP4Kbeta interacts with and modulates nuclear localization of the high-activity PtdIns5P-4-kinase isoform PIP4Kalpha. Biochem. J. *430*, 223–235.

Carricaburu, V., Lamia, K.A., Lo, E., Favereaux, L., Payrastre, B., Cantley, L.C., and Rameh, L.E. (2003). The phosphatidylinositol (PI)-5-phosphate 4-kinase type II enzyme controls insulin signaling by regulating PI-3,4,5-trisphosphate degradation. Proc. Natl. Acad. Sci. USA *100*, 9867–9872.

Choi, S., Thapa, N., Tan, X., Hedman, A.C., and Anderson, R.A. (2015). PIP kinases define PI4,5P_2signaling specificity by association with effectors. Biochim. Biophys. Acta *1851*, 711–723.

Choi, S., Hedman, A.C., Sayedyahossein, S., Thapa, N., Sacks, D.B., and Anderson, R.A. (2016). Agonist-stimulated phosphatidylinositol-3,4,5-trisphosphate generation by scaffolded phosphoinositide kinases. Nat. Cell Biol. *18*, 1324–1335.

Clarke, J.H., and Irvine, R.F. (2013). Evolutionarily conserved structural changes in phosphatidylinositol 5-phosphate 4-kinase (PI5P4K) isoforms are responsible for differences in enzyme activity and localization. Biochem. J. *454*, 49–57.

Clarke, J.H., Emson, P.C., and Irvine, R.F. (2008). Localization of phosphatidylinositol phosphate kinase IIgamma in kidney to a membrane trafficking compartment within specialized cells of the nephron. Am. J. Physiol. Renal Physiol. *295*, F1422–F1430.

De Leo, M.G., Staiano, L., Vicinanza, M., Luciani, A., Carissimo, A., Mutarelli, M., Di Campli, A., Polishchuk, E., Di Tullio, G., Morra, V., et al. (2016). Autophagosome-lysosome fusion triggers a lysosomal response mediated by TLR9 and controlled by OCRL. Nat. Cell Biol. *18*, 839–850.

Emerling, B.M., Hurov, J.B., Poulogiannis, G., Tsukazawa, K.S., Choo-Wing, R., Wulf, G.M., Bell, E.L., Shim, H.S., Lamia, K.A., Rameh, L.E., et al. (2013). Depletion of a putatively druggable class of phosphatidylinositol kinases inhibits growth of p53-null tumors. Cell *155*, 844–857.

Fellmann, C., Zuber, J., McJunkin, K., Chang, K., Malone, C.D., Dickins, R.A., Xu, Q., Hengartner, M.O., Elledge, S.J., Hannon, G.J., and Lowe, S.W. (2011). Functional identification of optimized RNAi triggers using a massively parallel sensor assay. Mol. Cell *41*, 733–746.

Fellmann, C., Hoffmann, T., Sridhar, V., Hopfgartner, B., Muhar, M., Roth, M., Lai, D.Y., Barbosa, I.A., Kwon, J.S., Guan, Y., et al. (2013). An optimized microRNA backbone for effective single-copy RNAi. Cell Rep. *5*, 1704–1713.

Fruman, D.A., Chiu, H., Hopkins, B.D., Bagrodia, S., Cantley, L.C., and Abraham, R.T. (2017). The PI3K Pathway in Human Disease. Cell *170*, 605–635.

Guo, J., Wenk, M.R., Pellegrini, L., Onofri, F., Benfenati, F., and De Camilli, P. (2003). Phosphatidylinositol 4-kinase type IIalpha is responsible for the phosphatidylinositol 4-kinase activity associated with synaptic vesicles. Proc. Natl. Acad. Sci. USA *100*, 3995–4000.

Gupta, A., Toscano, S., Trivedi, D., Jones, D.R., Mathre, S., Clarke, J.H., Divecha, N., and Raghu, P. (2013). Phosphatidylinositol 5-phosphate 4-kinase (PIP4K) regulates TOR signaling and cell growth during Drosophila development. Proc. Natl. Acad. Sci. USA *110*, 5963–5968.

Hinchliffe, K.A., Ciruela, A., Letcher, A.J., Divecha, N., and Irvine, R.F. (1999). Regulation of type IIalpha phosphatidylinositol phosphate kinase localisation by the protein kinase CK2. Curr. Biol. *9*, 983–986.

Hinchliffe, K.A., Giudici, M.L., Letcher, A.J., and Irvine, R.F. (2002). Type IIalpha phosphatidylinositol phosphate kinase associates with the plasma membrane via interaction with type I isoforms. Biochem. J. *363*, 563–570.

Homma, K., Terui, S., Minemura, M., Qadota, H., Anraku, Y., Kanaho, Y., and Ohya, Y. (1998). Phosphatidylinositol-4-phosphate 5-kinase localized on the plasma membrane is essential for yeast cell morphogenesis. J. Biol. Chem. *273*, 15779–15786.

Huttlin, E.L., Bruckner, R.J., Paulo, J.A., Cannon, J.R., Ting, L., Baltier, K., Colby, G., Gebreab, F., Gygi, M.P., Parzen, H., et al. (2017). Architecture of the human interactome defines protein communities and disease networks. Nature *545*, 505–509.

Itoh, T., Ijuin, T., and Takenawa, T. (1998). A novel phosphatidylinositol-5-phosphate 4-kinase (phosphatidylinositol-phosphate kinase IIgamma) is phosphorylated in the endoplasmic reticulum in response to mitogenic signals. J. Biol. Chem. *273*, 20292–20299.

Itzhak, D.N., Tyanova, S., Cox, J., and Borner, G.H. (2016). Global, quantitative and dynamic mapping of protein subcellular localization. eLife *5*, e16950.

Jenkins, G.H., Fisette, P.L., and Anderson, R.A. (1994). Type I phosphatidylinositol 4-phosphate 5-kinase isoforms are specifically stimulated by phosphatidic acid. J. Biol. Chem. *269*, 11547–11554.

Jones, D.R., Bultsma, Y., Keune, W.J., Halstead, J.R., Elouarrat, D., Mohammed, S., Heck, A.J., D'Santos, C.S., and Divecha, N. (2006). Nuclear PtdIns5P as a transducer of stress signaling: an in vivo role for PIP4Kbeta. Mol. Cell *23*, 685–695.

Kunz, J., Wilson, M.P., Kisseleva, M., Hurley, J.H., Majerus, P.W., and Anderson, R.A. (2000). The activation loop of phosphatidylinositol phosphate kinases determines signaling specificity. Mol. Cell *5*, 1–11.

Kunz, J., Fuelling, A., Kolbe, L., and Anderson, R.A. (2002). Stereo-specific substrate recognition by phosphatidylinositol phosphate kinases is swapped by changing a single amino acid residue. J. Biol. Chem. *277*, 5611–5619.

Lamia, K.A., Peroni, O.D., Kim, Y.B., Rameh, L.E., Kahn, B.B., and Cantley, L.C. (2004). Increased insulin sensitivity and reduced adiposity in phosphatidylinositol 5-phosphate 4-kinase beta-/- mice. Mol. Cell. Biol. *24*, 5080–5087.

Lundquist, M.R., Goncalves, M.D., Loughran, R.M., Possik, E., Vijayaraghavan, T., Yang, A., Pauli, C., Ravi, A., Verma, A., Yang, Z., et al. (2018). Phosphatidylinositol-5-Phosphate 4-Kinases Regulate Cellular Lipid Metabolism By Facilitating Autophagy. Mol. Cell *70*, 531–544.e9.

Mackey, A.M., Sarkes, D.A., Bettencourt, I., Asara, J.M., and Rameh, L.E. (2014). PIP4kγ is a substrate for mTORC1 that maintains basal mTORC1 signaling during starvation. Sci. Signal. *7*, ra104.

Manning, B.D., and Toker, A. (2017). AKT/PKB Signaling: Navigating the Network. Cell *169*, 381–405.

Muftuoglu, Y., Xue, Y., Gao, X., Wu, D., and Ha, Y. (2016). Mechanism of substrate specificity of phosphatidylinositol phosphate kinases. Proc. Natl. Acad. Sci. USA *113*, 8711–8716.

Nakatsu, F., Baskin, J.M., Chung, J., Tanner, L.B., Shui, G., Lee, S.Y., Pirruccello, M., Hao, M., Ingolia, N.T., Wenk, M.R., and De Camilli, P. (2012). PtdIns4P synthesis by PI4KIIIα at the plasma membrane and its impact on plasma membrane identity. J. Cell Biol. *199*, 1003–1016.

Niebuhr, K., Giuriato, S., Pedron, T., Philpott, D.J., Gaits, F., Sable, J., Sheetz, M.P., Parsot, C., Sansonetti, P.J., and Payrastre, B. (2002). Conversion of PtdIns(4,5)P(2) into PtdIns(5)P by the S.flexneri effector IpgD reorganizes host cell morphology. EMBO J. *21*, 5069–5078.

Pelossof, R., Fairchild, L., Huang, C.H., Widmer, C., Sreedharan, V.T., Sinha, N., Lai, D.Y., Guan, Y., Premsrirut, P.K., Tschaharganeh, D.F., et al. (2017). Prediction of potent shRNAs with a sequential classification algorithm. Nat. Biotechnol. *35*, 350–353.

Pendaries, C., Tronchère, H., Arbibe, L., Mounier, J., Gozani, O., Cantley, L., Fry, M.J., Gaits-Iacovoni, F., Sansonetti, P.J., and Payrastre, B. (2006). PtdIns5P activates the host cell PI3-kinase/Akt pathway during Shigella flexneri infection. EMBO J. *25*, 1024–1034.

Rameh, L.E., Tolias, K.F., Duckworth, B.C., and Cantley, L.C. (1997). A new pathway for synthesis of phosphatidylinositol-4,5-bisphosphate. Nature *390*, 192–196.

Ran, F.A., Hsu, P.D., Wright, J., Agarwala, V., Scott, D.A., and Zhang, F. (2013). Genome engineering using the CRISPR-Cas9 system. Nat. Protoc. *8*, 2281–2308.

Saito, K., Tolias, K.F., Saci, A., Koon, H.B., Humphries, L.A., Scharenberg, A., Rawlings, D.J., Kinet, J.P., and Carpenter, C.L. (2003). BTK regulates PtdIns-4,5-P2 synthesis: importance for calcium signaling and PI3K activity. Immunity *19*, 669–678.

Sharma, S., Mathre, S., Ramya, V., Shinde, D., and Raghu, P. (2019). Phosphatidylinositol 5 Phosphate 4-Kinase Regulates Plasma-Membrane PIP3 Turnover and Insulin Signaling. Cell Rep. *27*, this issue, 1979–1990.

Shim, H., Wu, C., Ramsamooj, S., Bosch, K.N., Chen, Z., Emerling, B.M., Yun, J., Liu, H., Choo-Wing, R., Yang, Z., et al. (2016). Deletion of the gene Pip4k2c, a novel phosphatidylinositol kinase, results in hyperactivation of the immune system. Proc. Natl. Acad. Sci. USA *113*, 7596–7601.

Sun, Y., Thapa, N., Hedman, A.C., and Anderson, R.A. (2013). Phosphatidylinositol 4,5-bisphosphate: targeted production and signaling. BioEssays *35*, 513–522.

van den Bout, I., and Divecha, N. (2009). PIP5K-driven PtdIns(4,5)P2 synthesis: regulation and cellular functions. J. Cell Sci. *122*, 3837–3850.

Wang, H., Sun, H.-Q., Zhu, X., Zhang, L., Albanesi, J., Levine, B., and Yin, H. (2015). GABARAPs regulate PI4P-dependent autophagosome:lysosome fusion. Proc. Natl. Acad. Sci. USA *112*, 7015–7020.

Weernink, P.A., Meletiadis, K., Hommeltenberg, S., Hinz, M., Ishihara, H., Schmidt, M., and Jakobs, K.H. (2004). Activation of type I phosphatidylinositol 4-phosphate 5-kinase isoforms by the Rho GTPases, RhoA, Rac1, and Cdc42. J. Biol. Chem. *279*, 7840–7849.

Wilcox, A., and Hinchliffe, K.A. (2008). Regulation of extranuclear PtdIns5P production by phosphatidylinositol phosphate 4-kinase 2alpha. FEBS Lett. *582*, 1391–1394.

Wiśniewski, J.R., Hein, M.Y., Cox, J., and Mann, M. (2014). A "proteomic ruler" for protein copy number and concentration estimation without spike-in standards. Mol. Cell. Proteomics *13*, 3497–3506.

Xie, Z., Chang, S.M., Pennypacker, S.D., Liao, E.Y., and Bikle, D.D. (2009). Phosphatidylinositol-4-phosphate 5-kinase 1alpha mediates extracellular calcium-induced keratinocyte differentiation. Mol. Biol. Cell *20*, 1695–1704.

STAR★METHODS

KEY RESOURCES TABLE

REAGENT or RESOURCE	SOURCE	IDENTIFIER
Antibodies		
PIP4K2A	Cell Signaling Technologies	Cat# 5527; RRID:AB_2722636
PIP4K2B	Cell Signaling Technologies	Cat# 9694; RRID:AB_2164572
PIP4K2C	Proteintech	Cat# 17077-1-AP; RRID:AB_2715526
PIP5K1A	Cell Signaling Technologies	Cat# 9693; RRID:AB_2164698
PIP5K1C	Abcam	Cat# Ab109192; RRID:AB_10862359
Rac1/2/3	Cell Signaling Technologies	Cat# 2465; RRID:AB_2176152
Lamp1	Cell Signaling Technologies	Cat# 15665; RRID:AB_2798750
pAKT-473	Cell Signaling Technologies	Cat# 4060; RRID:AB_2315049
pAKT-308	Cell Signaling Technologies	Cat# 13038; RRID:AB_2629447
AKT	Cell Signaling Technologies	Cat# 2920; RRID:AB_1147620
pPRAS40	Cell Signaling Technologies	Cat# 13175; RRID:AB_2798140
PRAS40	Cell Signaling Technologies	Cat# 2610; RRID:AB_916206
Beta-Actin	Abcam	Cat# Ab6276; RRID:AB_2223210
Tubulin	Abcam	Cat# Ab7291; RRID:AB_2241126
IRDye-secondary mouse	Li-Cor	Cat# 926-68070; RRID:AB_10956588
IRDye-secondary rabbit	Li-Cor	Cat# 926-32213;RRID:AB_621848
HRP-secondary mouse	Thermo Fisher Scientific	Cat# 45000679
HRP-secondary rabbit	Thermo Fisher Scientific	Cat# NA934-1ML
Alexa Fluor anti-mouse 568	Thermo Fisher Scientific	Cat# A10037
Alexa Fluor anti-rabbit 488	Thermo Fisher Scientific	Cat# A21206
Bacterial and Virus Strains		
Stbl3	Life Technologies	Cat# C737303
BL21	Life Technologies	Cat# C600003
Chemicals, Peptides, and Recombinant Proteins		
RIPA buffer	Sigma	Cat# R0278-500mL
Protease and phosphatase inhibitor	Thermo Fisher, Pierce	Cat# 88668
ECL substrate	Thermo Fisher, Pierce	Cat# 32106
Triton Lysis buffer	Cell Signaling Technologies	Cat# 9803
BCA Assay	Thermo Fisher	Cat# 23225
Precast gels	Life Technologies	Cat# NP0336BOX
DMEM	Corning	Cat# 10-013-CV
RPMI	Corning	Cat# 10-040-CV
Lipofectamine 2000	Life Technologies	Cat# 11668500
Opti-Mem	Life Technologies	Cat# 31985070
^{3}H inositol	Perkin Elmer	Cat# NET114A005MC
^{32}ATP	Perkin Elmer	Cat# BLU002A001MC
Dialyzed FBS	Life Technologies	Cat# 26400044
Inositol free DMEM	Thermo Fisher	Cat# ICN1642954
Glutamine	Life Technologies	Cat# 51985034
Dialyzed FBS	Life Technologies	Cat# 26400044
Inositol free DMEM	Thermo Fisher	Cat# ICN1642954
Glutamine	Life Technologies	Cat# 51985034
Ultima flo scintillation fluid	Perkin Elmer	Cat# 6013599

(*Continued on next page*)

Continued

REAGENT or RESOURCE	SOURCE	IDENTIFIER
Anti-HA magnetic beads	Pierce	Cat# 88836
Control magnetic beads	Cell signaling Technologies	Cat# 8726
Phosphatidylserine	Avanti	840032C
Phosphatidylinositol-4-phosphate	Avanti	Cat# 840151
Phosphatidylinositol-5-phosphate	Avanti	Cat# 850152P
IPTG	Technova	Cat# I3431
Glutathione Sepharose	Thermo Fisher	Cat# 45000285
TEV protease	Sigma	Cat# T4455-10KU
Fast SYBER green	Applied Biosystems	Cat# C0110820
Critical Commercial Assays		
RNEasy	QIAGEN	Cat# 74106
SuperScript VILO Mastermix	Life Technologies	Cat# 11755050
QuikChange	Agilent	Cat# 200522
BCA protein assay	Thermo Fisher	Cat# 23225
Mycoalert	Lonza	Cat# LT07318
Experimental Models: Cell Lines		
293T	Clontech	Cat# 632180
HeLa	ATCC	Cat# CCL-2
PaTu 8988t	DSMZ	Cat# ACC162
H1299	ATCC	Cat# CRL-5803
H1975	ATCC	Cat# CRL-5908
BJ	ATCC	Cat# CRL-2522
Oligonucleotides		
Table S3	This paper	N/A
Recombinant DNA		
LG3GEPIR	Fellmann et al., 2013	N/A
SGEP	Fellmann et al., 2013	N/A
SG3REPIR	This paper	N/A
SREN	This paper	N/A
pPIG-3xHA-empty	This paper	N/A
pPIG-3xHA-PIP4K2A	This paper	N/A
pPIG-3xHA-PIP4K2A-KD	This paper	N/A
pPIG-3xHA-PIP4K2C	This paper	N/A
pPIG 3xHA-PIP4K2C-VD	This paper	N/A
Software and Algorithms		
AutoQuant	Media Cybernetics	N/A
ImageQuant TL v8.1	GE	N/A
Prism	Graphpad	N/A
Accuri	BD Biosciences	N/A
Prism 7	Graphphad Prism Software	N/A
Other		
HiChrom Partisphere SAX HPLC 5 micron	VWR	Cat# 101946-560
Typhoon FLA 7000	GE	N/A

CONTACT FOR REAGENT AND RESOURCE SHARING

Further information and requests for resources and reagents should be directed to and will be fulfilled by the Lead Contact, Lewis C. Cantley (LCantley@med.cornell.edu).

EXPERIMENTAL MODEL AND SUBJECT DETAILS

Cell lines, authentication

Cell lines were purchased from ATCC and/or fingerprinted with the University of Arizona genetics core. Cells were tested to be mycoplasma free with Lonza Mycoalert.

Cell culture conditions

293T, HeLa, PaTu 8988t, and BJ cells were cultured using DMEM media supplemented with 10% FBS, glutamine and pyruvate. H1299 and H1975 cells were cultured in RPMI media.

METHOD DETAILS

Cell lysis and immunoblotting

Cells were lysed in RIPA buffer supplemented with 1 tablet of protease and phosphatase inhibitor. After incubation on ice for 20 minutes, lysates were cleared by centrifugation at 14,000 x g and supernatant was quantified using BCA assay. Lysates were subjected to SDS-PAGE using Novex NuPAGE system. Proteins were separated on 4%–12% Bis Tris Pre-Cast Gels 10% Bis Tris gels using MOPS buffer. Proteins were transferred to 0.45 μm nitrocellulose membranes at 350 mA for 1h. Membranes were blocked in 5% non-fat milk in TBST and incubated with primary antibody overnight: For chemi-luminescently detect antibody binding, membranes were blotted with HRP conjugated secondary antibodies. Membranes were developed using ECL solution, and exposed to film. For insulin signaling westerns, protocol was modified such that cells were lysed in triton buffer, IRDye secondary was used for Li-Cor Odyssey detection with quantification using Image Studio Lite software.

Generation of lentivirus, viral transduction

293T cells were used to generate lentivirus. Once cells were at 90%–95% confluence in a 10cm dish, transfection was performed with Opti-mem, Lipofectamine 2000, lentiviral vector, and accessory plasmids VSVG and Δ8.2. Virus supernatant was harvested 2 days and 3 days post transfection, then filtered and concentrated in an ultracentrifuge at 25,000 rpm for 120 minutes at 4°C.

Generation of cell lines with CRISPR knockout of PIP4K

CRISPR guides in pX458 were transfected in 293T cells. At 48-96 hours post transfection, GFP positive cells were single-cell sorted in 96-well plates using the Influx sorter at the WCMC Flow Cytometry Core. Two weeks later, wells were scored to contain single cell colony and expanded to screen for successful PIP4K2A/ PIP4K2B/ PIP4K2C knockout. Validation was performed by western blotting as well as PCR around each cut site.

Generation of cell lines with miR-E knockdown of PIP4K

LT3GEPIR vectors containing desired miR-E shRNA(s) were double digested downstream of existing shRNA(s) with EcoRI-HF/ MluI-HF and PCR purified (Fellmann et al., 2013). The miR-E sequence to be added was PCR amplified with Multi-sh-F and Multi-sh-R. PCR products were purified, double digested with BbsI/ MluI, and PCR purified once more. Ligations were performed with PCR product and open LT3GEPIR vectors using T4 ligase. Colonies were screened using miR-E-F. Primers listed in Table S3

Generation of mammalian and bacterial expression vectors

To generate vectors to express hairpin-resistant coding sequences for PIP4K isoforms, we cloned wild-type PIP4K2A and PIP4K2C into a lentiviral backbone with a PGK promoter. Next, we generated mutations in PIP4K cDNA using QuikChange to make kinase-dead variants and silent mutations in wobble positions for hairpin-resistant cDNA. Primers listed in Table S3. No wobble mutations were needed for PIP4K2C cDNA since all hairpins targeted the 3′ UTR. To generate PIP4K2C N-terminal mutants, Quikchange kit from Agilent (220521) was used and listed in Table S3.

Measurement of phosphoinositides with high performance liquid chromatography

Cellular phosphoinositides were metabolically labeled for 48 hours in inositol-free DMEM supplemented with glutamine,10% dialyzed FBS, and 10 μCi/ mL 3H myo-inositol. Cells were washed with PBS and then transferred on ice. Cells were killed and then harvested by scraping using 1.5 mL ice-cold aqueous solution (1M HCl, 5 mM Tetrabutylammonium bisulfate, 25 mM EDTA). 2 mL of ice cold MeOH and 4mL of CHCl3 were added to each sample. After ensuring each vial is tightly capped, samples were vortexed and then centrifuged at 1000 rpm for 5 min. If a significant intermediate layer was visible, sample were gently agitated and spun again, until there were predominately two clear layers. The organic layer (lower) was cleaned using theoretical upper, while the aqueous layer was cleaned using theoretical lower (theoretical upper and lower made by combining CHCl3: MeOH: aqueous solution in 8:4:3 v/v ratio). Organic phases were collected and dried under nitrogen gas. Lipids were deacylated using monomethylamine solution (47% Methanol, 36% of 40% Methylamine, 9% butanol, and 8% H2O, by volume). Samples were incubated at 55° for 1 hour and subsequently dried under nitrogen gas. To the dried vials, 1 mL of theoretical upper and 1.5 mL of theoretical lower were added (theoretical upper and lower made by combining CHCl3:MeOH:H2O in 8:4:3 v/v ratio). Samples were vortexed and spun at 1000rpm. The aqueous phase (upper) was collected and dried under nitrogen gas. Samples were resuspended in 150 μL Buffer

A (1mM EDTA), filtered and transferred to Agilent polypropylene tubes. Samples were analyzed by anion-exchange HPLC using Partisphere SAX column. The compounds were eluted with a gradient starting at 100% Buffer A (1mM EDTA) and increasing Buffer B (1mM EDTA, 1M NaH2PO4) over time: 0-1 min 100% Buffer A, 1-30 min 98% Buffer A/2% Buffer B, 30-31 min 86% Buffer A/ 14% Buffer B, 31-60 min 70% Buffer A/ 30% Buffer B, 60-80 min 34% Buffer A/ 66% Buffer B, 80-85 min 100% Buffer B, 85-120 min 100% Buffer A. Buffers were pumped at 1 mL/min through column. Eluate from the HPLC column flowed into an on-line continuous flow scintillation detector for isotope detection. The detector was set to observe events between 10 minutes and 85 minutes, with scintillation fluid flowing at 4 mL/min.

Measurement of phosphatidic acid using LCMS

Cellular lipids were extracted using same method described for phosphoinositide analysis. Lipids were dried and diluted with 113 μL of chloroform:methanol:water (73:23:3) mixture and filtered (0.45 μm) before analysis on an Agilent 6230 electrospray ionization–time-of-flight (ESI–TOF) MS coupled to an Agilent 1260 HPLC equipped with a Phenomenex Luna silica 3 μm 100 Å 5 cm x 2.0 mm column. LCMS analysis was performed using normal phase HPLC with a binary gradient elution system where solvent A was chloroform:methanol:ammonium hydroxide (85:15:0.5) and solvent B was chloroform:methanol:water:ammonium hydroxide (60:34:5:0.5). Separation was achieved using a linear gradient from 100% A to 100% B over 9 min. Phospholipid species were detected using a dual ESI source operating in positive mode, acquiring in extended dynamic range from m/z 100–1700 at one spectrum per second; gas temperature: 325°C; drying gas 10 L/min; nebulizer: 20 psig; fragmentor 300 V

Immunoprecipitation

293T cell lines expressing 3xHA empty vector or 3xHA-PIP5K1A were fixed for 10 minutes in 4% PFA, washed 3x with PBS, and lysed in lysis buffer (10mM Tris 7.4, 150 mM NaCl, 0.5 mM EDTA, 0.5% NP40) using probe sonicator for 2 minutes. Lysates were pre-cleared with control magnetic beads for 1 hour and 4° and Pierce magnetic anti-HA beads added for overnight incubation at 4°. Beads were washed 3x with lysis buffer and aliquots were added to sample buffer loading dye with beta mercaptoethanol, boiled, and run on SDS-page for immunoblotting.

Protein Purification

BL21 bacterial cells were transfected with pGEX vectors with PIP4K isoform coding sequence variants. Cells were grown in 1L of TB at 37° at 200rpm until 0.8 OD, at which point 500 uL of 1M IPTG was added. Cultures were shaken overnight at room temp for protein induction, and pelleted at 5000 g for 15 minutes. Cells were lysed (50 mM Tris pH 7.5, 500 mM NaCl, 10 mM MgCl2, 10% glycerol, DTT, lysozyme, protein/phosphatase inhibitors), sonicated for 1 minute (output 4, continuous duty cycle) and spun down at 10,000 g for 1 hour. Supernatant was kept for further purification and cleavage according to manufacturer's protocol using glutathione Sepharose beads.

In-vitro kinase assays

Cells were trypsinized and normalized for cell number. Cell pellets, or E.Coli purified proteins were resuspended in HNE buffer (20 mM HEPES pH 7.4, 100mM NaCl, 0.5mM EGTA), and sonicated in the presence of 32P-γ-ATP, and liposomes (10ug PS, 1ug PI(4)P in 30mM HEPES pH 7.4, 1mM EGTA). Liposome lipids were purchased from Avanti. Reactions were stopped by addition of 50uL of 4N HCL. To extract lipids, 100 μL of MeOH:CHCl3 (1:1) was added and samples were vortexed 2x 30 s. Samples were spun down at top speed for 2 min and the organic phase containing phosphatidylinositol lipids (bottom) were separated using thin-layer chromatography (TLC) using 1-propanol: 2N acetic acid (65:35 v/v). TLC plates were prepared ahead of time by coating with 1% Potassium Oxalate. Phosphorylated lipids were visualized by autoradiography on a GE Typhoon FLA 7000 and quantified using ImageQuant TL software.

GST Pulldown assays

GST tagged proteins were isolated as described above except that after washing, aliquots of beads with bound protein were added to 293T cell lysates generated by lysis in IP buffer (50 mM Tris-Cl pH 8.0, 150 mM NaCl, 1% NP-40, complete PI/Pis with EDTA) and spinning out DNA at 22,000xg x10min. These lysates and purified protein were incubated together at 4 degrees for 1 hour before the beads were again pelleted, washed with IP buffer three times, eluted with 2M NaCl, and analyzed by SDS-PAGE and western blot.

Fluorescence microscopy

293T cells were grown on glass coverslips pre-treated with poly-d-lysine. Adherent cell lines were rinsed with phosphate-buffered saline, pH 7.4 (PBS) and subsequently fixed/permeabilized in −20 MeOH for 20 minutes. After fixation, the cells were blocked for 30 minutes in blocking buffer (PBS with 3% BSA) and labeled with primary antibodies in blocking buffer for 1 hour at room temperature. Coverslips were washed three times with blocking buffer and incubated with Alexa Fluor-conjugated goat secondary antibodies in blocking buffer for 1 hour at room temperature. After incubation with secondary antibodies, coverslips were washed three times with PBS, once with water, and then mounted on a glass microscope slide with Prolong Gold with DAPI. The following primary antibodies were used: LAMP1. Alexa Fluor-conjugated secondary antibodies were used at 1:1000 (Thermo Scientific). Fluorescent and phase contrast images were acquired on a Nikon Eclipse Ti microscope equipped with an Andor Zyla sCMOS camera. Within

each experiment, exposure times were kept constant and in the linear range throughout. When using the 60x oil immersion objectives, stacks of images were taken and deconvoluted using AutoQuant.

qRT-PCR

Total RNA was prepared using RNeasy. cDNA was synthesized using Superscript Vilo and qRT-PCR performed utilizing Fast SYBR green and the Realplex Mastercycler. For a list of primers used see oligos in Table S3. Isolation of mRNA and qPCR was performed as follows. 200,000 cells were plated in 6-well plastic dishes. 24 hours later, the RNA in the lysates was extracted using the RNeasy protocol. The RNA was resuspended in 50 μL H_2O at a concentration of 1 μg/μL. cDNA was transcribed using the SuperScript Vilo. The sequences of the oligonucleotides used as primers in the PCR reactions are given in Table S3. The genes that were quantified here were previously shown to be regulated by TFEB

QUANTIFIICATION AND STATISTICAL ANALYSIS

Experiments were repeated with at least three biological replicates with the following exceptions: 1) Experiments in Figure S3 were performed once, and panels with error bars were performed with technical triplicates; 2) Experiments in Figures S4H–S4J were performed once. No samples were excluded from analysis. When comparing two groups, a two-tailed t test was used. P values are indicated in figure legends. When comparing greater than two groups, significance was calculated using ANOVA and Holm-Sidack post hoc test. Figure legends indicate which comparisons are significant, with respective p values.